Voltage-gated calcium channels trigger spontaneous glutamate release via nanodomain coupling

Byoung Ju Lee[§1,2], Che Ho Yang[§1,2], Seung Yeon Lee[1,2], Suk-Ho Lee[1,2,3,4], Yujin Kim*[2,3], Won-Kyung Ho*[1,2,3,4]

[1]Department of Biomedical Sciences, [2]Department of Physiology, [3]Neuroscience Research Institute, Seoul National University College of Medicine, [4]Department of Brain and Cognitive Science, Seoul National University College of Natural Science, Seoul, Korea

[§]These authors contributed equally to this work.

*Corresponding authors

Won-Kyung Ho and Yujin Kim

Department of Physiology, Seoul National University College of Medicine, 103 Daehak-ro, Jongno-gu, Seoul 03080, Korea

Tel: +82-2-740-8227, Fax: +82-2-763-9667.

E-mail: wonkyung@snu.ac.kr, km.y@snu.ac.kr

Declarations of interests: none

ABSTRACT

Neurotransmitter release occurs either synchronously to action potentials or spontaneously, yet whether molecular machineries underlying evoked and spontaneous release are identical, especially whether voltage-gated Ca^{2+} channels (VGCCs) can trigger spontaneous events has been in debate. To elucidate this issue, we characterized Ca^{2+} dependency of miniature excitatory postsynaptic currents (mEPSCs) in autaptic cultured hippocampal neurons. We found that 58 % mEPSC frequency was dependent on extracellular Ca^{2+} ($[Ca^{2+}]_o$), and Ca^{2+} cooperativity of spontaneous release was comparable to that of evoked release. Moreover, most (> 90 %) of $[Ca^{2+}]_o$-dependent mEPSCs was attributable to VGCCs. Coupling distance between VGCCs and Ca^{2+} sensors was estimated as tight for both spontaneous and evoked release (~22 nm). In hippocampal slices, VGCC-dependence on spontaneous release was also observed, but to a different extent, at different areas and ages. At the calyx of Held synapses, mEPSCs showed VGCC-dependence in type 1 mature synapses where VGCCs and Ca^{2+} sensors are tightly coupled, but not in immature synapses. These data strongly suggest that the distance between VGCCs and Ca^{2+} sensors is the key factor to determine VGCC dependence of spontaneous release.

INTRODUCTION

Synaptic transmission is a major mechanism for information processing in neural systems. Excitation of a neuron can be transmitted to postsynaptic neurons by means of neurotransmitter release triggered by action potentials (APs) in the presynaptic nerve terminals. However, neurotransmitter release also occurs spontaneously at resting state with low frequency around 0.01 Hz per synaptic bouton (Murthy and Stevens, 1999; Sara *et al.*, 2005). This type of synaptic communication has pivotal roles in synaptic structure and function, including synapse maturation and maintenance, homeostasis, and plasticity. In spite of physiological importance of spontaneous release, its molecular mechanisms are poorly understood.

Neurotransmitter release occurs when an increase in intracellular Ca^{2+} is detected by Ca^{2+} sensors at presynaptic terminals. During AP firing, Ca^{2+} influx mediated by VGCCs is captured by vesicular Ca^{2+} sensors, leading to synaptic vesicle fusion. Spontaneous release also involves Ca^{2+}-dependent processes, yet it is not clear whether extracellular Ca^{2+} ($[Ca^{2+}]_o$)-induced - spontaneous release utilizes the same Ca^{2+} sensors and sources with evoked release (Groffen *et al.*, 2010; Kavalali, 2015; Xu *et al.*, 2007; Xu *et al.*, 2009). In particular, the contribution of VGCCs to spontaneous release is controversial. It is generally accepted that stochastic VGCC activity is a major trigger of spontaneous release at inhibitory synapses (Goswami *et al.*, 2012; Williams *et al.*, 2012), yet the contribution of VGCCs was denied in many studies at excitatory synapses (Courtney *et al.*, 2018; Dai *et al.*, 2015; Tsintsadze *et al.*, 2017; Vyleta and Smith, 2011). It was proposed that spontaneous glutamate release is independent of Ca^{2+} influx via VGCCs, but tonically activated by calcium-sensing receptor (CaSR), which is a G-protein coupled receptor activated by $[Ca^{2+}]_o$ (Tsintsadze *et al.*, 2017; Vyleta and Smith, 2011). On the other hand, Ermolyuk et al. (2013) showed clear evidence that spontaneous glutamate release is triggered by local Ca^{2+} increases induced by stochastic opening of presynaptic VGCCs at resting state in hippocampal cultured neurons. These contradictory results may imply that Ca^{2+}-dependent spontaneous release was mediated by multiple Ca^{2+} sensors and multiple Ca^{2+} sources, and their relative contributions are distinct among different cell types and is regulated differentially by various cellular states or signaling mechanisms.

The coupling distance between Ca^{2+} sources and Ca^{2+} sensors of exocytosis is a key determinant of efficacy and speed of AP-triggered synaptic transmission (Eggermann *et al.*, 2012; Neher and Sakaba, 2008). In a nanodomain coupling, a single or a few numbers of Ca^{2+} channel openings would lead to brief and local rises in Ca^{2+} concentration and directly trigger synaptic vesicle fusion, so that tight coupling has functional advantages, including speed, temporal precision, and energy efficiency of synaptic transmission (Eggermann *et al.*, 2012; Schmidt *et al.*, 2013). On the other hand, loose

coupling enabled the control of initial release probability by fast endogenous Ca^{2+} buffers and the generation of facilitation by buffer saturation, thus providing the molecular framework for presynaptic plasticity (Vyleta and Jonas, 2014). The coupling configuration may also have implications for spontaneous release, but little information is available so far. The coupling distance can be probed using intracellular application of exogenous Ca^{2+} chelators with different kinetics, EGTA and BAPTA (Adler *et al.*, 1991; Neher, 1998), yet such experiments are not usually plausible in most neurons where presynaptic terminals are too small to be approached by patch pipettes. For this purpose, autaptic cultured neurons would be a useful system since application of exogenous Ca^{2+} chelators to presynaptic terminals is possible via somatic patch (Burgalossi *et al.*, 2012). In the present study, we used autaptic cultured hippocampal neurons to investigate the contribution of VGCCs to spontaneous release, and measured coupling distance between VGCCs and Ca^{2+} sensors. We also examined spontaneous glutamatergic responses at different subfields in the hippocampus, and found that VGCC dependence was variable at different areas. Studies on the calyx of Held synapses and our simulation data based on the experiment with exogenous Ca^{2+} chelators in culture hippocampal neurons revealed that the coupling distance between Ca^{2+} sensors and sources are the key determinant of VGCC-dependence of spontaneous glutamate release.

RESULTS

Ca^{2+} cooperativity of spontaneous glutamate release is similar to evoked release in autaptic hippocampal neurons

To measure spontaneous glutamate release at excitatory synapses, we recorded synaptic activities at resting state (-70 mV) under the whole-cell voltage clamp condition using pipette solutions containing 0.1 mM EGTA from hippocampal neurons grown isolated on astrocyte feeder islands at least for 3 weeks for synaptic maturation. (Fig. 1Aa). Neurons were identified as glutamatergic neurons firstly by the fast decay kinetics of synaptic currents (decay time constant: 3.02 ± 0.16 ms, N = 64), and then were confirmed by pharmacology. Postsynaptic currents which decayed within ~ 10 ms were not affected by 0.1 mM picrotoxin (PTX), but abolished by 10 μM CNQX (Fig. 1Ab). Since these activities were not affected by TTX, they were regarded as miniature excitatory postsynaptic currents (mEPSCs) representing spontaneous glutamate release (Fig. 1Ac). Frequencies of mEPSCs were variable among cells, ranging from 0.5 to 10 Hz (3.87 ± 0.18 Hz, N = 278). Hereafter, mEPSC frequency

obtained after applying any experimental conditions are normalized to the control level. When external Ca^{2+} was removed ($[Ca^{2+}]_o$ = 0 mM), mEPSC frequency decreased to 0.42 ± 0.03 (*N* = 13) (Figs. 1Ba, Bc), while inhibition of internal Ca^{2+} release via ryanodine receptors (RyRs) using ryanodine (RYN, 10 μM) reduced mEPSC frequency to 0.85 ± 0.04 (*N* = 6) (Figs. 1Bb, Bc). Ryanodine still reduced mEPSC frequency in Ca^{2+}-free condition (Supplementary Fig. 1), suggesting that internal and external Ca^{2+} mediate spontaneous release by independent mechanisms. Taken together, 58% and 15% of miniature events in autaptic cultured hippocampal neurons were attributable to $[Ca^{2+}]_o$-dependent and RyRs-dependent mechanisms, while 27% was Ca^{2+}-independent (Fig. 1Bd). mEPSC frequency changed according to $[Ca^{2+}]_o$ changes (top panel, Fig. 1C), with the slope of log-log plot for mEPSC frequency against $[Ca^{2+}]_o$ as 0.42 (black symbols and line, Fig. 1D), which is compatible to the value measured in cortical neurons, 0.63 (Vyleta and Smith, 2011). However, this slope represented underestimated Ca^{2+} cooperativity, since 42% of total mEPSCs is independent on $[Ca^{2+}]_o$. To obtain the actual Ca^{2+} cooperativity, we subtracted the $[Ca^{2+}]_o$-independent fraction and recalculated the slope. The result was 1.24 (red line, Fig. 1D), which turns out to be much higher than previous reports.

Our result challenges the view that spontaneous release would be governed by molecular machineries distinct from those for evoked release (Williams and Smith, 2018). To compare Ca^{2+} cooperativity of spontaneous and evoked release, we recorded evoked excitatory postsynaptic currents (eEPSCs) at different $[Ca^{2+}]_o$. Amplitude of eEPSC changed according to $[Ca^{2+}]_o$ as did mEPSC frequency (Fig. 1E). The slope of log-log plot for eEPSC amplitude against $[Ca^{2+}]_o$ was 1.84 (black line, Fig. 1F), which was smaller than that obtained in neuromuscular junction, 3.8 (Dodge and Rahamimoff, 1967), but compatible to that obtained in hippocampal synapses 1.77 (Vyleta and Jonas, 2014). Removal of $[Ca^{2+}]_o$ completely abolished eEPSC (Supplementary Fig. 2A), while ryanodine had no effect (Supplementary Fig. 2B), confirming that evoked release was entirely dependent on Ca^{2+} influx via VGCCs. Taken together, our data suggest that molecular machineries for Ca^{2+}-dependent spontaneous release may not be substantially different from those of evoked release.

VGCCs contribute to spontaneous glutamate release

Unlike evoked release, whether spontaneous glutamate release is mediated by presynaptic VGCCs remains controversial (Ermolyuk *et al.*, 2013; Vyleta and Smith, 2011). However, above results suggested the involvement of VGCCs in miniature events. To test this possibility, we examined the contribution of VGCCs to mEPSCs using blockers to specific VGCC subtypes. Blockade of P/Q-type

(with 0.1 μM ω-Agatoxin-IVA, Aga), N-type (with 0.1 μM ω-Conotoxin GVIA, Cono), and R-type VGCCs (with 0.3 μM SNX-482, SNX, or 100 μM $NiCl_2$) significantly decreased mEPSC frequency (Figs. 2Aa-c, C; Aga, 0.71 ± 0.02, *N* = 24, Cono, 0.73 ± 0.01, *N* = 18, SNX, 0.77 ± 0.06, *N* = 6, $NiCl_2$, 0.78 ± 0.02, *N* = 9). The mixture of Aga, Cono, and $NiCl_2$ (3-mix) decreased mEPSC frequency to 0.47 ± 0.02 (*N* = 10, Figs. 2Ad, C), suggesting that 91 % of $[Ca^{2+}]_o$-dependent mEPSCs is mediated by VGCCs. In the presence of 3-mix, changing $[Ca^{2+}]_o$ no longer affected mEPSC frequency (Fig. 2Ad), further confirming the role of VGCCs on $[Ca^{2+}]_o$-dependent miniature events.

One of the strong evidence that supports a lack of the VGCC contribution to spontaneous glutamate release is that Cd^{2+}, a non-selective VGCC blocker, has no significant effect (Dai *et al.*, 2015; Tsintsadze *et al.*, 2017; Vyleta and Smith, 2011). We measured mEPSCs in the presence of Cd^{2+} (100 μM), and found that mEPSC frequency was reduced to 0.70 ± 0.03 (*N* = 4, Figs. 2B, C). This was a significant decrease, yet smaller than that by 3-mix, suggesting that Cd^{2+} did not completely block VGCC-dependent spontaneous release. This concentration of Cd^{2+} was potent to abolish depolarization-induced Ca^{2+} currents (Supplementary Fig. 3, 0.04 ± 0.01, *N* = 3). Since VGCC blockade by Cd^{2+} is voltage-dependent and not as effective at hyperpolarizing potential (Swandulla and Armstrong, 1989), Cd^{2+}may not be suitable to assess VGCC dependency at resting membrane potential (RMP). We confirmed that mEPSC amplitudes were not changed by any VGCC blockers (Fig. 2D).

To further understand the role of VGCCs in glutamate release, we compared the effects of each VGCC blocker on eEPSCs and mEPSCs. All VGCC blockers decreased eEPSC amplitude significantly (Figs. 2Ea-c, F), which was associated with an increase in paired pulse ratio (Fig. 2G). The contribution of P/Q-, N-, and R-type VGCCs were 65 %, 40 %, and 40 %, respectively (Fig. 2H), which were slightly different from their contribution to mEPSCs (P/Q, 53 %; N, 49 %; R, 42 %; Fig. 2H). The linear sum of the contribution of the three VGCCs exceeds 100 % (145 % for eEPSCs and 144 % for mEPSCs, Fig. 2H), suggesting that the contribution of each type of VGCC is not entirely independent.

Nanodomain coupling between Ca^{2+} sources and Ca^{2+} sensors for both spontaneous and evoked glutamate release

Another factor that determines the molecular machineries for exocytosis is how tightly Ca^{2+} sources,

VGCCs in this case, is coupled with vesicular Ca^{2+} sensors. The distance between VGCCs and Ca^{2+} sensors can be probed using exogenous Ca^{2+} chelators with different kinetics, EGTA and BAPTA (Adler *et al.*, 1991; Neher, 1998). When the channel-sensor coupling is very tight, so called nanodomain coupling, the fast Ca^{2+} buffer such as BAPTA, but not the slow Ca^{2+} buffer such as EGTA, can interfere exocytosis, while when the coupling is loose, EGTA as well as BAPTA can interfere (Adler *et al.*, 1991; Neher, 1998). To examine whether vesicular Ca^{2+} sensors that operate for spontaneous and evoked release are identical or distinct, we measured mEPSC frequency and eEPSC amplitude from the same cells with intracellular EGTA or BAPTA (Fig. 3A). eEPSCs were recorded every 20 s starting immediately after patch break-in, while mEPSCs were recorded for 10 s in between eEPSCs (Fig. 3A). Sequential recordings for eEPSCs and mEPSCs continued until the effects of EGTA or BAPTA perfusion reached steady state. We performed these experiments in the presence of ryanodine to exclude the effects of exogenous buffer on RyR-dependent mEPSCs, which was mediated by loose coupling with Ca^{2+} sensors (Supplementary Fig. 4). Changes in eEPSCs or mEPSCs were small with 5 mM EGTA (black circles, Figs. 3Bb, Cb), while a significant reduction was induced in both eEPSC amplitude and mEPSC frequency with 5 mM BAPTA (blue circles, Figs. 3Bb, Cc). Differential effects of EGTA and BAPTA suggest tight coupling between VGCCs and Ca^{2+} sensors both for spontaneous and evoked release. To estimate the distance between Ca^{2+} sensors and VGCCs, we recorded eEPSCs and mEPSCs with different concentrations of BAPTA and EGTA (Figs. 3Da, Db). Then, we subtracted $[Ca^{2+}]_o$-independent portion (0.26 ± 0.02, N = 5, in 5 mM EGTA and 0.25 ± 0.03, N = 7, in 5 mM BAPTA) from the measured mEPSC frequencies (circles) to obtain changes in $[Ca^{2+}]_o$-dependent mEPSCs, which were re-normalized to the first point. The resulting curves (red lines) were superimposed to the changes in eEPSC amplitude for comparison (Figs. 3Da, Db). eEPSC amplitude (symbols) and mEPSC frequency (lines) decreased as the concentration of each buffer increased (Figs. 3Da, Db) with time course and magnitude indistinguishable between eEPSCs and mEPSCs at all concentrations tested (Fig. 3D). The distance between Ca^{2+} sources and sensors was estimated by fitting these values to the following equation (see Methods).

$$\text{Mini frequency ratio} = \exp[n\,(-r/\lambda_0\,(\sqrt{(1+(P_{b,1}/P_0)\,x)} - 1))].$$

, where x = [EGTA] or [BAPTA] in mM; n = power dependence of vesicle release on $[Ca^{2+}]c$, λ_0 = length constant of calcium microdomain in the presence of endogenous buffer (B_0) alone; P_0 and $P_{b,1}$ are buffer products (k_{on} [B]) of B_0 and 1 mM EGTA or BAPTA, respectively. Since decreases in mEPSC frequency and eEPSC amplitude by EGTA and BAPTA were almost identical, we pooled the data for fitting. The best fit was obtained at r = 22 nm where n = 1.62 and P_0 = 3000 (Fig. 3E, mEPSCs, triangles; eEPSCs, circles). These data suggest that both spontaneous and evoked glutamate release is triggered by VGCCs via nanodomain coupling in cultured hippocampal neurons.

Contribution of VGCCs to spontaneous glutamate release in hippocampal neurons at different subfields and calyx of Held synapses

Previous studies reported that only spontaneous GABA release, but not spontaneous glutamate release, is mediated by VGCCs (Courtney *et al.*, 2018; Tsintsadze *et al.*, 2017; Vyleta and Smith, 2011). These results, inconsistent with ours, may imply that the contribution of VGCCs to glutamatergic miniature events may vary among different cell types or synapses. To investigate this possibility, we examined the effect of $[Ca^{2+}]_o$ removal and VGCC blockers on mEPSCs in pyramidal neurons in CA1 and CA3 hippocampus (CA1-PCs and CA3-PCs) and granule cells in hippocampal dentate gyrus (DG-GCs) of 3-week-old rats. mEPSCs frequency was distinct between groups in a range of 1 and 5 (Supplementary Fig. 5), while the $[Ca^{2+}]_o$-dependent portion was not substantially different among neurons at different hippocampal areas (42 ~ 46 %, Figs. 4Aa-c, D), yet slightly smaller than that observed in hippocampal cultured neuron (58 %, Fig. 1Bd). In contrast, the effect of 3-mix on mEPSCs were various among neurons at different areas. mEPSC frequency was hardly changed by 3-mix in DG-GCs (Figs. 4Ba, D), but significantly reduced in CA3-PCs (Figs. 4Bb, D). In CA1-PCs, mEPSC frequency did not change in 3-mix (Figs. 4Bc, D), yet it was significantly reduced when basal mEPSC frequency was increased by high external K^+ (5 mM; Figs. 4Ca, D), showing that VGCCs got involved in spontaneous release when RMP is depolarized. We additionally found that 3-mix significantly reduced mEPSC frequency in CA1 neurons from 4-week-old rats (Figs. 4Cb, D), suggesting that VGCC-dependence on spontaneous release can be modulated by developmental stages.

Developmental changes of coupling distance between VGCCs and vesicular Ca^{2+} sensors from loose (~100 nm) to tight coupling (~20 nm) were well characterized in glutamatergic synapses onto principal cells of the medial nucleus of the trapezoid body (MNTB), which is called the calyx of Held synapses (Fedchyshyn and Wang, 2005; Wang *et al.*, 2009). To investigate whether coupling distance affected the contribution of VGCCs to spontaneous release, we recorded mEPSCs from presynaptic calyces in acute auditory brainstem slices obtained from rats at different ages in the presence of 3-mix or absence of $[Ca^{2+}]_o$. mEPSC frequency at immature synapses was $[Ca^{2+}]_o$-dependent, yet not mediated by VGCCs (3-mix, 0.95 ± 0.03; 0 mM $[Ca^{2+}]_o$, 0.34 ± 0.05, N = 5, Figs. 5A, D), which is consistent with previous reports (Dai *et al.*, 2015; Tsintsadze *et al.*, 2017). At mature synapses, on the other hand, mEPSC frequency was significantly reduced by 3-mix (0.63 ± 0.08, N = 12, Figs. 5B, D), while the $[Ca^{2+}]_o$-dependent portion of mEPSCs was comparable to that at young synapses (Fig. 5D). These data suggest that VGCCs were engaged to spontaneous release during synaptic maturation by

tightening of coupling between VGCCs and Ca^{2+} sensors.

Recent studies showed that mature calyx of Held synapses are morphologically heterogeneous, grouped into three types depending on the number of swellings (Grande and Wang, 2011), and that type 1 calyces contain synaptic vesicles tightly coupled to VGCCs (~14 nm), whereas type 3 calyces harbor a mixture of loosely (30 - 50 nm) and tightly coupled vesicles (Fekete *et al.*, 2019). We noted that the potency of 3-mix on mEPSC frequency at mature synapses varied widely (Fig. 5C), and suspected that this heterogeneous response could be related to the morphological heterogeneity (Grande and Wang, 2011). Thus, we grouped mature calyces into three types as previously reported (Grande and Wang, 2011), and examined the relationship between the variable sensitivity of mEPSC to VGCC blockade and synaptic morphology. Among 12 calyces, there were 4 calyces in type 1 (Fig. 5Ea; left) and 4 calyces in type 3 (Fig. 5Ea; right), and their mEPSC frequency was not significantly different (type 1, 1.99 ± 0.5; type 3, 1.57 ± 0.31 Hz). However, only type 1 calyces showed a dramatic reduction of mEPSC frequency in 3-mix (Figs. 5Eb, Ec), while type 3 calyces did not show any apparent changes (Figs. 5Eb, Ec). Thus, our data suggest that tight coupling of VGCCs and vesicular Ca^{2+} sensors is prerequisite for VGCC-dependent spontaneous release.

Relative contributions of $[Ca^{2+}]_o$-dependent and $[Ca^{2+}]_o$-independent spontaneous release at different cell types or synapses that we examined here are summarized in Figure 5F. The fraction of $[Ca^{2+}]_o$-dependent miniature events (light and dark blue) was not much different (0.42 ~ 0.69), while the VGCC contribution to $[Ca^{2+}]_o$-dependent release showed a wide variation (0.07 ~ 0.92, Fig. 5G) depending on brain area, maturation stages, or synaptic morphology. Taken together, these data suggest the relationship between the VGCC contribution to spontaneous release and tight coupling between VGCCs and Ca^{2+} sensors.

DISCUSSION

While Ca^{2+} influx through VGCCs in presynaptic axon terminals is critical for evoked synaptic transmitter release, the role of VGCCs in spontaneous glutamate release still remains controversial (Williams and Smith, 2018). In the present study, we found that spontaneous glutamate release is dependent on Ca^{2+} influx via P/Q-, N-, and R-type VGCCs in autaptic cultured hippocampal neurons. Moreover, estimation of the coupling distance between VGCCs and Ca^{2+} sensors by fitting the buffered Ca^{2+} diffusion model to the effects of two different Ca^{2+} chelators on mEPSCs and eEPSCs showed tight coupling configuration for both spontaneous and evoked release (~22 nm), suggesting

general molecular machineries for VGCC-dependent exocytosis in both types of release. The contribution of VGCCs to miniature events is variable in the hippocampus and the calyx of Held depending on areas and developmental stages. Among those, VGCC-dependence was most significant in mature type 1 calyx of Held synapses where the coupling distance between Ca^{2+} sensors and Ca^{2+} sources is known to be very tight (~14 nm) (Fekete *et al.*, 2019). These data suggest that the coupling distance between Ca^{2+} sensors and Ca^{2+} sources is a critical factor in determining the contribution of VGCCs to spontaneous release. The physical distance between presynaptic VGCCs and Ca^{2+} sensors, which may vary depending on cell types and developmental states (Baur *et al.*, 2015; Bornschein *et al.*, 2019; Taschenberger *et al.*, 2002; Wang *et al.*, 2008), has been considered as an important feature of the synapses that determines the characteristics of AP-triggered neurotransmission (Eggermann *et al.*, 2012; Rebola *et al.*, 2019). Our study highlights the role of coupling distance in regulating spontaneous neurotransmission.

It has been of a great interest whether molecular machineries of Ca^{2+}-dependent spontaneous release operate as those of evoked release do. Autaptic cultured neurons serve as ideal preparation to investigate this issue, since mEPSCs and eEPSCs are originated from the same set of presynaptic terminals, and thus, direct comparison of the two are allowed. Our results obtained from autaptic hippocampal neurons showed remarkable similarities in VGCC-dependence as well as Ca^{2+} cooperativity between spontaneous and evoked release, suggesting that VGCCs could be the Ca^{2+} source for both of the two release, which is consistent with a previous study (Ermolyuk *et al.*, 2013). Likewise, Ca^{2+} sensors involved in the two release may not be different. A recent study showed that synaptic vesicles for miniature events are originated from the recycling pool, which is also the source of evoked release (Hua *et al.*, 2010). The role of VGCCs in spontaneous glutamate release was, however, denied in many other studies (Courtney *et al.*, 2018; Dai *et al.*, 2015; Tsintsadze *et al.*, 2017; Vyleta and Smith, 2011), and a lack of VGCC contribution was regarded to represent fundamental differences in molecular machineries between spontaneous and evoked release (Williams and Smith, 2018). We found a variability of the extent of VGCC contribution to mini events at different synapses in brain slices, which could be the reason for conflicting previous reports. We confirmed the previous report showing that VGCC did not contribute to mini events in CA1 neurons (Babiec and O'Dell, 2018), but additionally showed that VGCC contribution was revealed by increasing $[K^+]_o$ from 2.5 mM to 5 mM (Figs. 4Ca, D), implying that local Ca^{2+} increase mediated by VGCC opening is increased to the level for triggering spontaneous release at depolarized RMP. These data suggest that a lack of VGCC contribution to mini events is not due to the difference in molecular machineries, but due to insufficient coupling. We showed that in autaptic cultured hippocampal neurons that have tight coupling between Ca^{2+} sources and sensors, spontaneous glutamate release is indeed mediated by VGCCs, with similar Ca^{2+} cooperativity to evoked release.

Unlike glutamatergic synapses, it is generally accepted that spontaneous release at GABAergic synapses is mediated mainly by VGCCs (Williams *et al.*, 2012; Williams and Smith, 2018). A low-affinity Ca^{2+} sensor synaptotagmin 1 (Syt1) was shown to mediate spontaneous as well as evoked release (Courtney *et al.*, 2018; Xu *et al.*, 2009) and VGCC blockers affected Syt1-dependent spontaneous release in GABAergic synapses, but not in glutamatergic synapses (Courtney *et al.*, 2018). These findings were regarded to represent divergence in the release machinery between GABAergic and glutamatergic neurons (Courtney *et al.*, 2018), but our study showed that VGCC-dependent spontaneous release occurred in certain glutamatergic synapses. It is interesting to note similar features underlying spontaneous GABA release reported previously (Williams *et al.*, 2012; Williams and Smith, 2018) and our results. Tight coupling regime was used both in VGCC-dependent GABAergic mini events in cultured neocortical neurons (Williams *et al.*, 2012) and glutamatergic mini events in autaptic cultured hippocampal neurons (Fig. 2) and at type 1 calyx of Held synapses (Fig. 5). Thus, these results suggest that the tightness of coupling between VGCCs and Ca^{2+} sensors could be a universal mechanism underlying VGCC-dependence of spontaneous release regardless of the type of synapses. At GABAergic synapses where coupling is generally tight (Bucurenciu *et al.*, 2010; Hefft and Jonas, 2005), VGCCs would play a critical role in spontaneous release, whereas at glutamatergic synapses, VGCCs could participate at certain synapses that have tight coupling configuration, but not at most synapses. mEPSCs in CA1 neurons did not show VGCC-dependence in the control conditions, but VGCC dependence emerged at high $[Ca^{2+}]_o$ (Courtney *et al.*, 2018) or depolarized RMP (Fig. 4Ca), suggesting that loose coupling can be overcome when Ca^{2+} influx or intracellular $[Ca^{2+}]$ is increased. However, such interpretation may not be generalized to all synapses. In dentate gyrus granule cells, a major fraction of VGCC-dependent spontaneous GABA release is generated at the terminals of CCK-expressing interneurons (Goswami *et al.*, 2012), which are known to have loose coupling between VGCCs and sensors (Ali and Todorova, 2010; Daw *et al.*, 2009; Hefft and Jonas, 2005). We showed that VGCC contribution to mEPSCs is significant in CA3 neurons (Fig. 4Bb), but there is no experimental evidence that inputs to CA3 neurons have tight VGCC to Ca^{2+} sensor coupling. In fact, mossy fiber-CA3 synapses are known as loose-coupling synapses with coupling distance 73 - 80 nm (Vyleta and Jonas, 2014). These results may suggest the presence of other factors that determine the contribution of VGCCs to spontaneous release than coupling distance. Possibly, the number of VGCCs at active zone may affect the VGCC contribution. To further understand the underlying mechanisms, information about the VGCCs-to-vesicle topography in the active zone of different synapses is required.

Experiments at different subfields in the hippocampus and the calyx of Held synapses in different developmental stages revealed similar $[Ca^{2+}]_o$-dependency regardless of VGCC dependence, implying the existence of VGCC-independent component. Under the circumstances whereby stochastic opening of VGCCs cannot trigger glutamate release at hippocampal subfields, about half of

spontaneous glutamate release is mediated by $[Ca^{2+}]_o$-dependent mechanisms (Figs. 4A, D). We did not identify the nature of $[Ca^{2+}]_o$-dependent mechanisms other than VGCCs in the present study. Activation of the Ca^{2+} sensing receptor (CaSR), a G-protein coupled receptor activated by extracellular Ca^{2+}, was proposed to stimulate spontaneous release in glutamatergic neurons (Vyleta and Smith, 2011). However, results obtained using CaSR knockout neurons revealed that CaSR activation mediates only ~30% of spontaneous release and CaSR-dependent release decreases, not increases, as $[Ca^{2+}]_o$ increases (Vyleta and Smith, 2011). Such response did not conform the typical response of spontaneous release upon changing $[Ca^{2+}]_o$. Possibly, multiple Ca^{2+} sources that are involved in regulating resting Ca^{2+} levels, such as internal Ca^{2+} source (Carter *et al.*, 2002; Emptage *et al.*, 2001; Sharma and Vijayaraghavan, 2003) or TRPC (Peters *et al.*, 2010; Shoudai *et al.*, 2010), may contribute to spontaneous release by activating Doc2, a high-affinity Ca^{2+} sensor exclusively for spontaneous release (Groffen *et al.*, 2010), yet the relationship between these sources and Doc2 remains to be uncovered. Taken together, various Ca^{2+} sources would participate in spontaneous release at different cells and conditions.

Materials and Methods

Autaptic Neuronal culture

All preparations were carried out under the animal welfare guideline of Seoul National University (SNU), and approved by IACUC of SNU. Primary cultures of rat hippocampal neurons were prepared as described previously with slight adaptations (Bekkers and Stevens, 1991). Briefly, hippocampal neurons and astrocytes were obtained from Sprague-Dawley (SD) rats according to the protocols approved by the Seoul National University Institutional Animal Care and Use Committee. Astrocyte cultures were prepared from the Sprague-Dawley rat cortices P0 - P1 and grown for 10 days in 100-mm culture dish in glial medium [minimum essential medium (MEM; Invitrogen) supplemented with 0.6 % glucose, 1 mM pyruvate, 2 mM GlutaMAX-I (Invitrogen), 10 % horse serum (HS; Invitrogen), and 1 % penicillin-streptomycin (PS; Invitrogen)] before plating on the sprayed microisland coverslips in 30-mm petri dishes. 2 - 3 days before neurons being added in sprayed microisland dishes, astrocytes were removed from the 100-mm culture dish using trypsin-EDTA (Invitrogen) and plated on the microisland coverslips at a density of 60,000 cells/dish. Hippocampi from P0 - P1 SD rats were dissected in Hank's balanced salt solution (Invitrogen), digested with papain (Worthington, Freehold, NJ, USA), and then triturated with a polished half-bore Pasteur pipette. Immediately after removing glia medium in 30-mm dishes of microisland-shaped astrocytes, hippocampal neurons were added at a density of 6,000 cells/dish and were grown in neurobasal medium supplemented with B27 and glutamax (Invitrogen).

Hippocampal Slice Preparation

Hippocampal slices were prepared from 3-week-old (P17 - 21) or 4-week-old (P23 - 30) Sprague-Dawley rats. After anaesthetized by inhalation with 5% isoflurane, rats were decapitated and the brain was quickly removed and chilled in an ice-cold high-magnesium cutting solution containing the following (in mM): 110 choline chloride, 25 $NaHCO_3$, 20 glucose, 2.5 KCl, 1.25 NaH_2PO_4, 1 sodium pyruvate, 0.5 $CaCl_2$, 7 $MgCl_2$, 0.57 ascorbate (pH 7.3 bubbled with 95 % O_2 - 5 % CO_2; osmolarity ~300 mOsm. The isolated brain was glued onto the stage of a vibrating blade microtome (VT1200S, Leica Microsystems) and 300 μm-thick transverse hippocampal slices were cut. The slices were incubated at 34°C for 30 min in artificial cerebrospinal fluid (aCSF) containing the following (in mM): 125 NaCl, 25 $NaHCO_3$, 20 glucose, 2.5 KCl, 1.25 NaH_2PO_4, 1 sodium pyruvate, 2 $CaCl_2$, 1 $MgCl_2$, 0.57 ascorbate, bubbled with 95 % O_2 - 5 % CO_2, and thereafter maintained at room temperature until required.

Calyx of Held Brain Slice Preparation

Transverse brainstem slices (300 µm thick) were prepared from 7 to 18-day-old (P7 - 9, immature pre-hearing onset; P16 - 18, mature post-hearing onset) Sprague-Dawley rats. The standard extracellular solution contained (in mM) 125 NaCl, 2.5 KCl, 25 glucose, 25 $NaHCO_3$, 1.25 NaH_2PO_4, 0.4 ascorbic acid, 3 myoinositol, 2 Na-pyruvate and 2 $CaCl_2$, 1$MgCl_2$ (pH 7.4, bubbled with 95 % O_2 - 5 % CO_2; osmolarity ~320 mOsm). For slicing, $CaCl_2$ and $MgCl_2$ were changed to 0.5 and 2.5 mM, respectively. Slices were incubated at 34°C for 30 min in the extracellular solution and thereafter maintained at room temperature until required.

Electrophysiology

For recordings in autaptic cultured neurons, cells were visualized with an Olympus IX70 inverted microscope. Whole-cell voltage- or current-clamp recordings from hippocampal autaptic pyramidal neurons were performed at room temperature and continuously perfused with extracellular solution consisting of following composition (in mM): 135 NaCl, 2.5 KCl, 2 $CaCl_2$, 1 $MgCl_2$, 10 glucose, 10 HEPES, 0.1 EGTA, pH 7.3 adjusted with NaOH (295 - 300 mOsm), and maintained at 0.5 - 1 ml min^{-1}. All recordings were done at least 23 days after neurons were plated on coverslips. The internal pipette solution for recording mEPSCs and resting membrane potential (RMP) was used K-gluconate based solution.

For recordings in hippocampal slices, slices were transferred to an immersed recording chamber continuously perfused with oxygenated aCSF using a peristaltic pump (Gilson). CA3 or CA1 pyramidal cells were visualized using an upright microscope equipped with differential interference contrast optics (BX51WI, Olympus). Whole-cell voltage- or current-clamp recordings were performed at 32 ± 1°C and the rate of aCSF perfusion was maintained at 1 - 1.5 ml min^{-1}. For high $[K^+]_o$ experiments, NaCl was reduced to maintain osmolarity. Recordings were made in somata with an EPC-10 amplifier (HEKA Electonik, Lambrecht/Pfalz, Germany). Signals were low-pass filtered at 5 kHz (low-pass Bessel filter) and sampled at 10 kHz. Series resistance (R_s) was monitored, and only recordings with R_s remained constant (<30% change during a recording) were used. R_s was compensated to 50 - 70 %. The data were analyzed using IGOR software (Wavemetrics, Lake Oswego, OR, USA). Patch electrodes were pulled from borosilicate glass capillaries to a resistance between 3 and 4 MΩ when filled with pipette solution. The internal pipette solution for recording miniature excitatory postsynaptic currents (mEPSCs) contained the following composition (in mM): 130 Cs-methanesulfate, 8 NaCl, 4 MgATP, 0.3 NaGTP, 10 HEPES, 0.1 EGTA, pH 7.3 adjusted with

CsOH (295 - 300 mOsm). For RMP recording, K-gluconate was substituted for Cs-methanesulfate, and pH was adjusted with KOH.

The mEPSCs of hippocampal slices or hippocampal autapses were recorded at holding potential of -70 mV. 0.5 μM TTX and 0.1 mM picrotoxin (PTX) was added during recordings in acute slices. Events exceeding 6 - 7 pA within a specified interval of three to four digitized points (0.5 - 0.8 ms) that showed a single exponential decay time course were identified as mEPSC. The rise time of mEPSC indicated the 20 - 80 % rise time. mEPSC frequency esd measured within 20 s bins. Synaptic activities were recorded at a holding potential of -70 mV. eEPSCs were recorded every 20 s after applying depolarization pulses from -70 to 0 mV for 2 ms. From the continuous recordings at -70 mV without stimulations, toxins and chemicals were typically applied for 5 - 20 min until a constant effect was observed.

For recording from calyx of Held synapses, brainstem slices were transferred to a recording chamber in an upright microscope and whole-cell patch-clamp recordings were made at room temperature using an EPC10/2 amplifier (HEKA, Pfalz, Germany). Postsynaptic cells were whole-cell voltage clamped at a holding voltage of -70 mV using a pipette (3.0 - 3.5 MΩ) solution containing the following (in mM): 140 Cs-gluconate, 20 tetraethylammonium (TEA)-Cl, 5 Na_2-phosphocreatine, 4 MgATP, 0.3 Na_2GTP, 20 HEPES, 10 EGTA at pH 7.4 (adjusted with CsOH). Experiments were discarded when series resistance exceeded 10 MΩ (range, 4 - 10 MΩ). After recordings of mEPSCs from postsynaptic MNTB neurons were complete, pairing presynaptic calyces terminals were filled with Alexa Fluor 488 for less than 1 min using another whole-cell pipette, and then the presynaptic pipette was carefully withdrawn to allow resealing of the presynaptic membrane. We immediately took high-resolution confocal *Z*-stack images of the recorded calyces, from which the 3D structure of the calyx was reconstructed using FIJI (Grande and Wang, 2011). For this procedure, presynaptic patch electrodes with resistance of 3 to 4 MΩ contained the following (in mM): 140 K-gluconate, 20 KCl, 10 HEPES, 5 Na_2-phosphocreatine, 4 Mg-ATP, 0.3 Na-GTP, 0.5 EGTA, and 0.25 Alexa Fluor 488 hydrazide (Invitrogen) with pH adjusted at 7.4.

Drugs

ω-Agatoxin-IVA, ω-Conotoxin GVIA, SNX-482, TTX, and ryanodine were purchased from Alomone Labs (Jerusalem, Israel). All other chemicals were purchased from Sigma (St. Louis, MO, USA). Toxin stock solutions were made at 1000-fold concentration with distilled water and stored at -20°C.

Estimation of the distance between Ca^{2+} sensors and VGCCs

Extensive theoretical studies assert that buffered calcium diffusion from open calcium channels make calcium microdomain of tens of micromolar concentration (Neher, 1998). Assuming that free buffer concentration does not change very much owing to rapid diffusional replacement of Ca^{2+}-bound buffer molecules with free buffer, the spatial profile of $[Ca^{2+}]$ as a function of distance from an open calcium channel (r) is given by:

$$[Ca^{2+}](r) = i_{Ca} / (4\ F\ D_{Ca}\ r)\ \exp(-r/\lambda)$$

, where i_{Ca} = calcium current; F = Faraday constant; D_{Ca} = diffusion constant of Ca^{2+} in cytosol.

Therefore, the ratio of $[Ca^{2+}]$ at a given distance from a Ca^{2+} channel (r) before and after the addition of BAPTA is as follows:

$$\text{Ca ratio} = \exp(-r/\lambda_b) / \exp(-r/\lambda_0)$$

, where λ_0 and λ_b are the length constants before and after BAPTA was added, respectively. Since the length constant, λ, in the presence of free calcium buffer [B] with Ca^{2+} binding rate constant, k_{on}, is given by

$$\lambda = \sqrt{D_{Ca} / (k_{on}\ [B])}$$

. Inserting this equation into the Ca ratio equation, we have dependence of calcium ratio as a function of $[BAPTA]_{total}$ (x, in mM) as follows:

$$\text{Ca ratio} = \exp[-r/\lambda_0\ (\sqrt{(1+ (P_{b,1}/P_0)\ x)} - 1)]$$

, where λ_0 = length constant in the presence of endogenous buffer (B_0) alone; P_0 and $P_{b,1}$ are buffer products (k_{on} [B]) of B_0 and 1 mM BAPTA, respectively. Finally, assuming that only the calcium influx through a calcium channel (or cluster) nearest to a vesicle is relevant to its release, and that glutamate release has the n-th power dependence on $[Ca^{2+}]$, the ratio of release (R_{rls}) before and after adding BAPTA has the relationship:

$$R_{rls} = \exp[\ n\ (-r/\lambda_0\ (\sqrt{(1+ (P_{b,1}/P_0)\ x)} - 1))]$$

. The n values for miniature and evoked EPSCs were obtained from Fig. 1D and 1F. $P_{b,1}$ is calculated as 300 $mM^{-1}ms^{-1}$ considering that k_{on} of BAPTA = 400 $mM^{-1}ms^{-1}$, and $[Ca^{2+}]_{rest}$ = 80 nM. Fitting the above equation to the plot of evoked or miniature EPSC frequency as a function of $[BAPTA]_{total}$ with setting r/λ_0 and P_0 as free parameters, we estimated the distance of vesicles from the calcium source (r).

Statistical analysis

Data were are expressed as the mean ± SEM, where *N* represents the number of cells studied. Statistical analysis was performed using IgorPro (version 6.1, WaveMetrics, Lake Oswego, OR, USA) and OriginPro (version 9.0, OriginLab Corp., Northampton, MA, USA). Significant differences between the experimental groups were analyzed using independent or paired Student's *t*-tests. $P<0.05$ was considered statistically significant.

FIGURE LEGENDS

Fig. 1. Ca^{2+} co-operativity for spontaneous glutamate release and evoked release. (Aa) A representative image of hippocampal neurons in an autaptic culture system with a patch electrode on the somata for whole-cell patch clamp. (Ab) Top. A representative trace of mEPSC in the presence of PTX and CNQX. Bottom. left*:* an enlarged trace of a single mEPSC. middle: bar graph indicating rise or decay time constant for mEPSC. Rise time was 0.53 ± 0.02 ms (*N* = 62). right: histogram representing a mEPSC frequency distribution for total number of cells used in the present study. (Ac) A representative trace of mEPSC in 0.5 μM TTX (*N* = 7, frequency; 0.99 ± 0.01 compared to control, amplitude; 15.57 ± 1.3 *vs* 15.63 ± 1.3 pA). (Ba, Bb) Top. Representative traces of mEPSC frequency during removal of external Ca^{2+} or RYN application, respectively. Bottom. An average time course of mEPSC frequency. In each time course plot, the upper solid line indicates an application point for 0 Ca^{2+} or RYN. (Bc) A bar graph for average effects of external Ca^{2+}-free (*N* = 13, 0.42 ± 0.03, $P < 0.001$) or RYN (*N* = 6, 0.85 ± 0.04) on mEPSC frequency. (Bd) Pie chart evaluating the relative contribution of Ca^{2+} -dependent (blue), -independent (grey) or internal Ca^{2+} release (magenta) to mEPSC. (Ca, Cb) Top. Representative traces of mEPSC frequency changing of $[Ca^{2+}]_o$. Bottom. An average time course of mEPSC frequency (0.5 *vs* 8 mM Ca^{2+}; 0.56 ± 0.02 *vs* 2.94 ± 0.24, *N* = 28 *vs* 17, compared to 2 mM Ca^{2+}). (D) A log-log plot for mEPSC frequency against $[Ca^{2+}]_o$. The slope of mEPSC frequency was 0.42 which was fitted from 2 mM to lower concentration (black circles and dash line). To overcome underestimated slope value, external Ca^{2+}-free fraction from the measured mEPSC frequency was subtracted and the slope was recalculated (red circles and dashed line, Slope; 1.24). (Ea, Eb) Top. Representative traces of eEPSC changing of $[Ca^{2+}]_o$. Bottom. An average time course of eEPSC amplitude (0.5 *vs* 4 mM Ca^{2+}; 0.11 ± 0.02 *vs* 1.42 ± 0.04, compared to 2 mM Ca^{2+}, *N* = 16 *vs* 6, $P < 0.001$). (F) A log-log plot for the eEPSC amplitude against $[Ca^{2+}]_o$. The slope of the eEPSC amplitude was 1.84 which was fitted from 2 mM to lower concentration (black circles and dash line). All data are mean ± S.E.M., $^*P < 0.05$, $^{***}P < 0.001$, single group mean *t*-test or paired *t*-test (Ac); n.s. = not significant.

Fig. 2. VGCCs contribute to spontaneous and evoked glutamate release. (Aa-c, B) Top. Representative traces of mEPSC frequency in the presence of Aga, Cono, SNX, $NiCl_2$ or $CdCl_2$, respectively. Bottom. An average time course of mEPSC frequency. The top solid line indicates an application point for each VGCC blocker. (Ad) Average time courses (bottom) of mEPSC frequency

with 3-mix (Aga + Cono + $NiCl_2$) in 2 mM Ca^{2+} or changing of $[Ca^{2+}]_o$ (2 Ca^{2+}, 0.47 ± 0.02, *N* = 10; 0.5 Ca^{2+}, 0.47 ± 0.01, *N* = 5; 8 Ca^{2+}, 0.48 ± 0.02, *N* = 4, compared to control). (C, D) Bar graphs showing normalized mEPSC frequency (Aga, blue, 0.71 ± 0.02, *N* = 24, *P* < 0.001; Cono, red, 0.73 ± 0.01, *N* = 18; SNX, green, 0.77 ± 0.06, *N* = 6; $NiCl_2$, green, 0.78 ± 0.02, *N* = 9; $CdCl_2$, 0.70 ± 0.03, *N* = 4, compared to control; C) and amplitude (D). (Ea-c) Top. Representative traces of 1st eEPSC amplitude in the presence of Aga, Cono, SNX, $NiCl_2$ or $CdCl_2$, respectively. Bottom. An average time course of 1st eEPSC amplitude. (F) A bar graph showing effects of individual blockers on the 1st eEPSC amplitude (Aga, 0.35 ± 0.03, *N* = 12; Cono, 0.6 ± 0.02, *N* = 37; $NiCl_2$, 0.6 ± 0.03, *N* = 18, compared to control). (G) A bar graph showing effects of individual blockers on paired-pulse ratio (PPR) (Aga, 0.97 ± 0.04 *vs* 1.31 ± 0.04; Cono, 0.97 ± 0.04 *vs* 1.16 ± 0.06; $NiCl_2$, 0.93 ± 0.04 *vs* 1.09 ± 0.09, compared to control, paired *t* test). (H) A chart for the VGCC contribution to mEPSC (pale bar) or eEPSC (solid bar). The arithmetic sum of the contributions of each blocker exceeded 1 both in spontaneous and evoked release. All data are mean ± S.E.M., **P* < 0.05, ****P* < 0.001, single group mean *t* test or paired *t*-test (G); n.s. = not significant.

Fig. 3. Nanodomain coupling between Ca^{2+} sources and Ca^{2+} sensors for both spontaneous and evoked glutamate release. (A) Experimental scheme for sequential recordings of eEPSCs and mEPSCs from same cells. (Ba, Ca) Representative traces for the comparison of eEPSCs and mEPSC between immediately patch break-in and 10 min after patch in presence of 5 mM EGTA (black) or 5 mM BAPTA (blue) in intracellular solution. (Bb) An average time course of the eEPSC amplitude. The magnitude of reduction at steady state and the time course (τ) were 0.75 ± 0.06 *vs* 0.07 ± 0.05 and 1146 ± 85 s *vs* 221 ± 9.2 s (5 EGTA *vs* 5 BAPTA; *N* = 5 *vs* 7). (Cb, Cc) Average time courses of mEPSC frequency (circles). Once reached the steady state, extracellular solution was changed to Ca^{2+}-free medium to exclude Ca^{2+}-independent mechanism for mEPSC. Extracellular Ca^{2+}-dependent mEPSC frequency (lines) was calculated by subtracting the Ca^{2+}-independent portion from the recorded mEPSC frequency. The magnitude of reduction at steady state and the time course (τ) were 0.74 ± 0.05 *vs* 0.07 ± 0.03 and 1004 ± 107 s *vs* 277 ± 12.3 s. (Da, Db) Average sequential time plots for mEPSC frequency (lines) or the eEPSC amplitude (symbols) in the presence of varying concentration of Ca^{2+} chelator in intracellular solution (20 EGTA, eEPSC vs mEPSC, 0.51 ± 0.03 *vs* 0.52 ± 0.04 and 307.7 ± 10.1 s *vs* 363.6 ± 13.4 s, *N* = 4; 0.5 BAPTA, 0.46 ± 0.07 *vs* 0.41 ± 0.05 and 588.2 ± 37.6 s *vs* 625 ± 40 s, *N* = 5; 1 BAPTA, 0.31 ± 0.04 *vs* 0.35 ± 0.03 and 357.1 ± 11.8 s *vs* 335.8 ± 14.3 s, *N* = 8). (E) Concentration-effect curves for BAPTA (blue) and EGTA (black). The steady state values were normalized by the value of just after whole-cell patch break-in configuration. All data

are mean ± S.E.M.

Fig. 4. Contribution of VGCCs to spontaneous glutamate release in acute hippocampal slices. (Aa-c) Top. Representative traces of mEPSC frequency during removal of external Ca^{2+} recording from DG (Aa), CA3 (Ab) and CA1 (Ac). Bottom. An average time course of mEPSC frequency. (Ba-c) Top. Representative traces of mEPSC frequency applying 3-mix at different synapses, respectively. Bottom. An average time course of mEPSC frequency. (Ca) Top. Representative traces of mEPSC frequency applying high concentration of K^+ and 3-mix from CA1 (3 wks). Bottom. An average time course of mEPSC frequency. (Cb) Top. Representative traces of mEPSC frequency applying 3-mix at CA1 (4 wks). Bottom. An average time course of mEPSC frequency. (D) A bar graph of average effects of 0 Ca^2, 3-mix, or 5 mM $[K^+]_o$ on mEPSC frequency. Average effects of 3-mix were 1.13 ± 0.1 from DG (N = 4), 0.7 ± 0.01 from CA3 (N = 13), 0.96 ± 0.02 from CA1 (3 wks, N = 30) and 0.8 ± 0.03 from CA1 (4 wks, N = 9). Average effects of 5 mM $[K^+]_o$ were 1.44 ± 0.1 (N = 7) and 3-mix (1.07 ± 0.02) at CA3-CA1 synapses (3 wks). All data are mean ± S.E.M., *P < 0.05, **P < 0.01, ***P < 0.001, single group mean t-test or paired t-test (H); n.s. = not significant.

Fig. 5. Contribution of VGCCs to spontaneous glutamate release in calyx of Held synapses in acute brain slices. (Aa, Ba) Representative traces of mEPSC frequency applying 3-mix and Ca^{2+}-free external solution at immature (Aa; P7 - 9) and mature (Ba; P16 - 18) calyx of Held synapses. (Ab, Bb) Average time courses of normalized mEPSC frequency. (C) A bar graph of mEPSC frequency at immature and mature synapses (immature, 0.31 ± 0.06 Hz, N = 5; mature, 1.85 ± 0.21 Hz, N = 12). (D) A bar graph of average effects of 3-mix (immature, 0.95 ± 0.03; mature, 0.63 ± 0.08) and external Ca^{2+}-free condition (immature, 0.34 ± 0.05; mature, 0.26 ± 0.08). (Ea) 3D reconstruction images of type 1 (left) and type 3 (right) calyces filled with Alexa-488. (Eb) Average time courses of normalized mEPSC frequency applying 3-mix (red; type 1, black; type3). (Ec) A bar graph showing normalized mEPSC frequency applying 3-mix (type 1, 0.53 ± 0.13; type 3, 0.84 ± 0.11). (F) A bar graph of relative contribution to Ca^{2+}-dependence on spontaneous glutamate release. (Autapse, 0.58; CA3, 0.42; CA1, 3 wks, 0.44; CA1, 4 wks, 0.42; calyx, Imm, 0.6; calyx, Mat, 0.69). (G) A bar graph of VGCC contribution to Ca^{2+}-dependence on spontaneous glutamate release (Autapse, 0.92; CA3, 0.58; CA1, 3 wks, 0.07; CA1, 4 wks, 0.46; calyx, Imm, 0.09; calyx, Mat, 0.67). All data are mean ± S.E.M., *P < 0.05, **P < 0.01, ***P < 0.001, single group mean t-test; n.s. = not significant.

Acknowledgement

This research was supported by the National Research Foundation grants from the Korean Ministry of Science and ICT (2020R1A2B5B02002070 to W.-K. Ho).

Data statement

The datasets generated and/or analyzed during the current study are available from the corresponding authors on reasonable request.

REFERENCES

Adler, E.M., Augustine, G.J., Duffy, S.N., Charlton, M.P., 1991. Alien intracellular calcium chelators attenuate neurotransmitter release at the squid giant synapse. *J. Neurosci.*, 1496–1507

Ali, A.B., Todorova, M., 2010. Asynchronous release of GABA via tonic cannabinoid receptor activation at identified interneuron synapses in rat CA1. *Eur. J. Neurosci.* 31, 1196-1207.

Babiec, W.E., O'Dell, T.J., 2018. Novel Ca^{2+}-dependent mechanisms regulate spontaneous release at excitatory synapses onto CA1 pyramidal cells. *J. Neurophysiol.* 119, 597-607.

Baur, D., Bornschein, G., Althof, D., Watanabe, M., Kulik, A., Eilers, J., Schmidt, H., 2015. Developmental tightening of cerebellar cortical synaptic influx-release coupling. *J. Neurosci.* 35, 1858-1871.

Bekkers, J.M., Stevens, C.F., 1991. Excitatory and inhibitory autaptic currents in isolated hippocampal neurons maintained in cell cultur. *Proc. Nati. Acad. Sci. U.S.A.* 88, 7834-7838.

Bornschein, G., Eilers, J., Schmidt, H., 2019. Neocortical high probability release sites are formed by distinct Ca^{2+} channel-to-release sensor topographies during development. *Cell Rep.* 28, 1410-1418 e1414.

Bucurenciu, I., Bischofberger, J., Jonas, P., 2010. A small number of open Ca^{2+} channels trigger transmitter release at a central GABAergic synapse. *Nat. Neurosci.* 13, 19-21.

Burgalossi, A., Jung, S., Man, K.N., Nair, R., Jockusch, W.J., Wojcik, S.M., Brose, N., Rhee, J.S., 2012. Analysis of neurotransmitter release mechanisms by photolysis of caged Ca^{2+} in an autaptic neuron culture system. *Nat. Protoc.* 7, 1351-1365.

Carter, A.G., Vogt, K.E., Foster, K.A., Regehr, W.G., 2002. Assessing the role of calcium-induced calcium release in short-term presynaptic plasticity at excitatory central synapses. *J. Neurosci.* 22, 21–28.

Courtney, N.A., Briguglio, J.S., Bradberry, M.M., Greer, C., Chapman, E.R., 2018. Excitatory and inhibitory neurons utilize different Ca^{2+} sensors and sources to regulate spontaneous release. *Neuron* 98, 977-991.

Dai, J., Chen, P., Tian, H., Sun, J., 2015. Spontaneous vesicle release Is not tightly coupled to voltage-gated calcium channel-mediated Ca^{2+} influx and is triggered by a Ca^{2+} sensor other than synaptotagmin-2 at the juvenile mice calyx of Held synapses. *J. Neurosci.* 35, 9632-9637.

Daw, M.I., Tricoire, L., Erdelyi, F., Szabo, G., McBain, C.J., 2009. Asynchronous transmitter release from cholecystokinin-containing inhibitory interneurons is widespread and target-cell independent. *J. Neurosci.* 29, 11112-11122.

Dodge, F.A.J., Rahamimoff, R., 1967. Co-operative action of calcium ions in transmitter release at the neuromuscular junction. *J. Physiol.* 193, 419-432.

Eggermann, E., Bucurenciu, I., Goswami, S.P., Jonas, P., 2012. Nanodomain coupling between Ca^{2+} channels and sensors of exocytosis at fast mammalian synapses. *Nat. Rev. Neurosci.* 13, 7-21.

Emptage, N.J., Reid, C.A., Fine, A., 2001. Calcium stores in hippocampal synaptic boutons mediate short-term plasticity, store-operated Ca^{2+} entry, and spontaneous transmitter release. *Neuron* 29, 197-208.

Ermolyuk, Y.S., Alder, F.G., Surges, R., Pavlov, I.Y., Timofeeva, Y., Kullmann, D.M., Volynski, K.E., 2013. Differential triggering of spontaneous glutamate release by P/Q-, N- and R-type Ca^{2+} channels. *Nat. Neurosci.* 16, 1754-1763.

Fedchyshyn, M.J., Wang, L.Y., 2005. Developmental transformation of the release modality at the calyx of Held synapse. *J. Neurosci.* 25, 4131-4140.

Fekete, A., Nakamura, Y., Yang, Y.M., Herlitze, S., Mark, M.D., DiGregorio, D.A., Wang, L.Y., 2019. Underpinning heterogeneity in synaptic transmission by presynaptic ensembles of distinct morphological modules. *Nat. Commun.* 10, 826-841.

Goswami, S.P., Bucurenciu, I., Jonas, P., 2012. Miniature IPSCs in hippocampal granule cells are triggered by voltage-gated Ca^{2+} channels via microdomain coupling. *J. Neurosci.* 32, 14294-14304.

Grande, G., Wang, L.Y., 2011. Morphological and functional continuum underlying heterogeneity in the spiking fidelity at the calyx of Held synapse in vitro. *J. Neurosci.* 31, 13386-13399.

Groffen, A.J., Martens, S., Arazola, R.D., Cornelisse, L., Lozovaya, N., Jong, A.P.H., Goriounova, N.A., Habets, R.L.P., Takai, Y., Borst, J.G., Brose, N., McMahon, H.T., Verhage, M., 2010. Doc2b is a high-affinity Ca^{2+} sensor for spontaneous neurotransmitter release. *Science* 327, 1614-1618.

Hefft, S., Jonas, P., 2005. Asynchronous GABA release generates long-lasting inhibition at a hippocampal interneuron-principal neuron synapse. *Nat. Neurosci.* 8, 1319-1328.

Hua, Y., Sinha, R., Martineau, M., Kahms, M., Klingauf, J., 2010. A common origin of synaptic vesicles undergoing evoked and spontaneous fusion. *Nat. Neurosci.* 13, 1451-1453.

Kavalali, E.T., 2015. The mechanisms and functions of spontaneous neurotransmitter release. *Nat. Rev. Neurosci.* 16, 5-16.

Murthy, V.N., Stevens, C.F., 1999. Reversal of synaptic vesicle docking at central synapses. *Nat. Neurosci.* 2, 503-507.

Neher, E., 1998. Usefulness and limitations of linear approximations to the understanding of Ca^{2+} signals. *Cell Calcium* 24, 345-357.

Neher, E., Sakaba, T., 2008. Multiple roles of calcium ions in the regulation of neurotransmitter release. *Neuron* 59, 861-872.

Peters, J.H., McDougall, S.J., Fawley, J.A., Smith, S.M., Andresen, M.C., 2010. Primary afferent activation of thermosensitive TRPV1 triggers asynchronous glutamate release at central neurons. *Neuron* 65, 657-669.

Rebola, N., Reva, M., Kirizs, T., Szoboszlay, M., Lorincz, A., Moneron, G., Nusser, Z., DiGregorio, D.A., 2019. Distinct nanoscale calcium channel and synaptic vesicle topographies contribute to the diversity of synaptic function. *Neuron* 104, 693-710 e699.

Sara, Y., Virmani, T., Deak, F., Liu, X., Kavalali, E.T., 2005. An isolated pool of vesicles recycles at

rest and drives spontaneous neurotransmission. *Neuron* 45, 563-573.

Schmidt, H., Brachtendorf, S., Arendt, O., Hallermann, S., Ishiyama, S., Bornschein, G., Gall, D., Schiffmann, S.N., Heckmann, M., Eilers, J., 2013. Nanodomain coupling at an excitatory cortical synapse. *Curr. Biol.* 23, 244-249.

Sharma, G., Vijayaraghavan, S., 2003. Modulation of presynaptic store calcium induces release of glutamate and postsynaptic firing. *Neuron* 38, 929-939.

Shoudai, K., Peters, J.H., McDougall, S.J., Fawley, J.A., Andresen, M.C., 2010. Thermally active TRPV1 tonically drives central spontaneous glutamate release. *J. Neurosci.* 30, 14470-14475.

Swandulla, D., Armstrong, C.M., 1989. Calcium channel block by cadmium in chicken sensory neurons. *Proc. Nati. Acad. Sci. U.S.A.* 86, 1736-1740.

Taschenberger, H., Leão, R.M., Rowland, K.C., Spirou, G.A., von Gersdorff, H., 2002. Optimizing synaptic architecture and efficiency for high-frequency transmission *Neuron* 36, 1127-1143.

Tsintsadze, T., Williams, C.L., Weingarten, D.J., von Gersdorff, H., Smith, S.M., 2017. Distinct actions of voltage-activated Ca^{2+} channel block on spontaneous release at excitatory and inhibitory central synapses. *J. Neurosci.* 37, 4301-4310.

Vyleta, N.P., Jonas, P., 2014. Loose coupling between Ca^{2+} channels and release sensors at a plastic hippocampal synapse. *Science* 343, 665-670.

Vyleta, N.P., Smith, S.M., 2011. Spontaneous glutamate release is independent of calcium influx and tonically activated by the calcium-sensing receptor. *J. Neurosci.* 31, 4593-4606.

Wang, L.Y., Fedchyshyn, M.J., Yang, Y.M., 2009. Action potential evoked transmitter release in central synapses: insights from the developing calyx of Held. *Mol. Brain* 2, 1-11.

Wang, L.Y., Neher, E., Taschenberger, H., 2008. Synaptic vesicles in mature calyx of Held synapses sense higher nanodomain calcium concentrations during action potential-evoked glutamate release. *J. Neurosci.* 28, 14450-14458.

Williams, C., Chen, W., Lee, C.H., Yaeger, D., Vyleta, N.P., Smith, S.M., 2012. Coactivation of multiple tightly coupled calcium channels triggers spontaneous release of GABA. *Nat. Neurosci.* 15, 1195-1197.

Williams, C.L., Smith, S.M., 2018. Calcium dependence of spontaneous neurotransmitter release. *J. Neurosci. Res.* 96, 335-347.

Xu, J., Mashimo, T., Sudhof, T.C., 2007. Synaptotagmin-1, -2, and -9: Ca^{2+} sensors for fast release that specify distinct presynaptic properties in subsets of neurons. *Neuron* 54, 567-581.

Xu, J., Pang, Z.P., Shin, O.H., Sudhof, T.C., 2009. Synaptotagmin-1 functions as a Ca^{2+} sensor for spontaneous release. *Nat. Neurosci.* 12, 759-766.

Fig. 1.

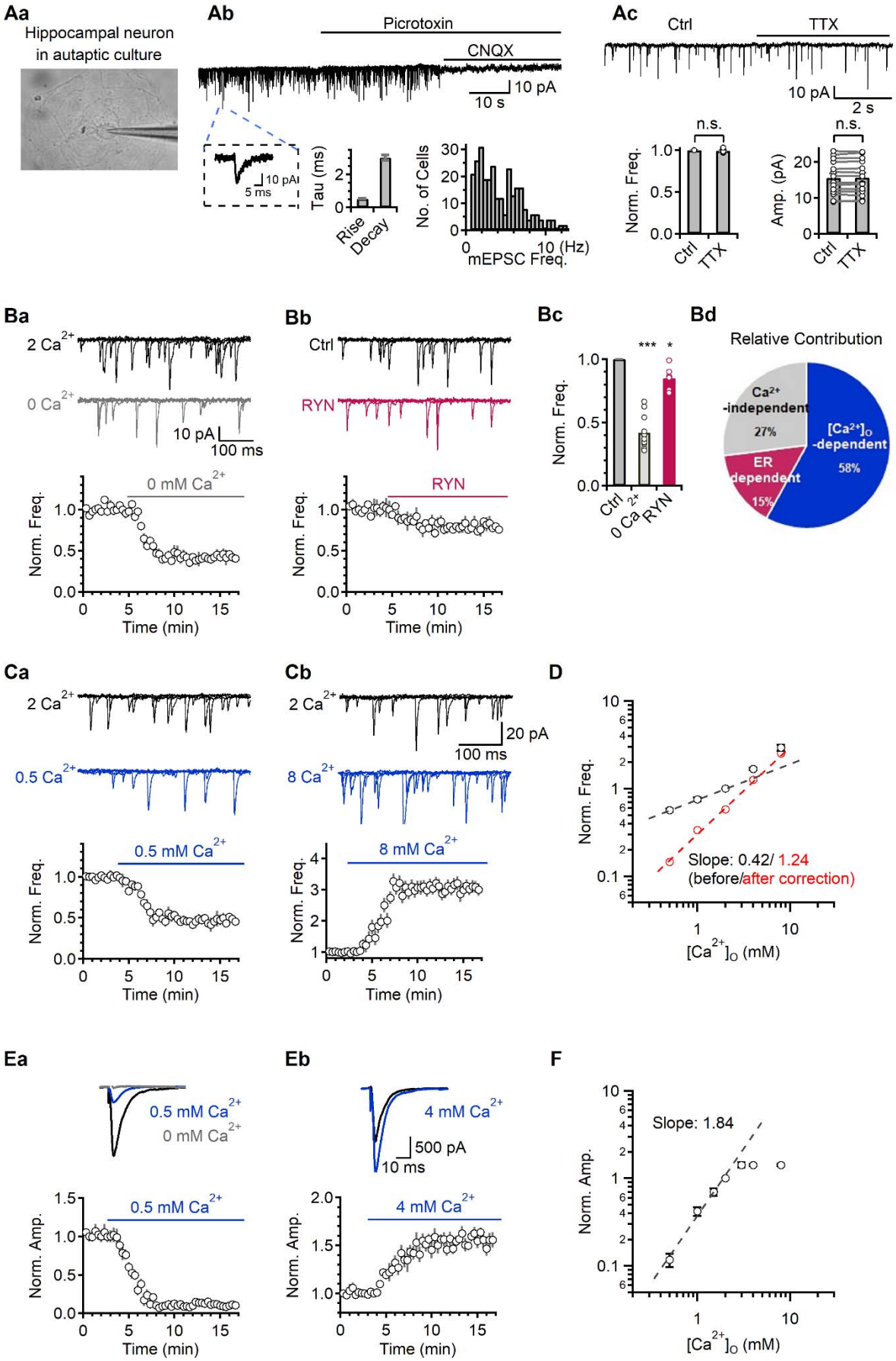
Aa
Hippocampal neuron in autaptic culture
Ab
Picrotoxin
CNQX
10 pA
10 s
10 pA
5 ms
Tau (ms)
Rise
Decay
No. of Cells
mEPSC Freq.
10 (Hz)
Ac
Ctrl
TTX
10 pA
2 s
n.s.
Norm. Freq.
Amp. (pA)
Ba
2 Ca2+
0 Ca2+
10 pA
100 ms
0 mM Ca2+
Norm. Freq.
Time (min)
Bb
Ctrl
RYN
Bc
***
*
Bd
Relative Contribution
Ca2+ -independent 27%
[Ca2+]O -dependent 58%
ER dependent 15%
Ca
0.5 Ca2+
0.5 mM Ca2+
Cb
20 pA
8 Ca2+
8 mM Ca2+
D
Slope: 0.42/ 1.24
(before/after correction)
[Ca2+]O (mM)
Ea
0.5 mM Ca2+
0 mM Ca2+
Norm. Amp.
Eb
4 mM Ca2+
500 pA
10 ms
F
Slope: 1.84

Fig. 2.

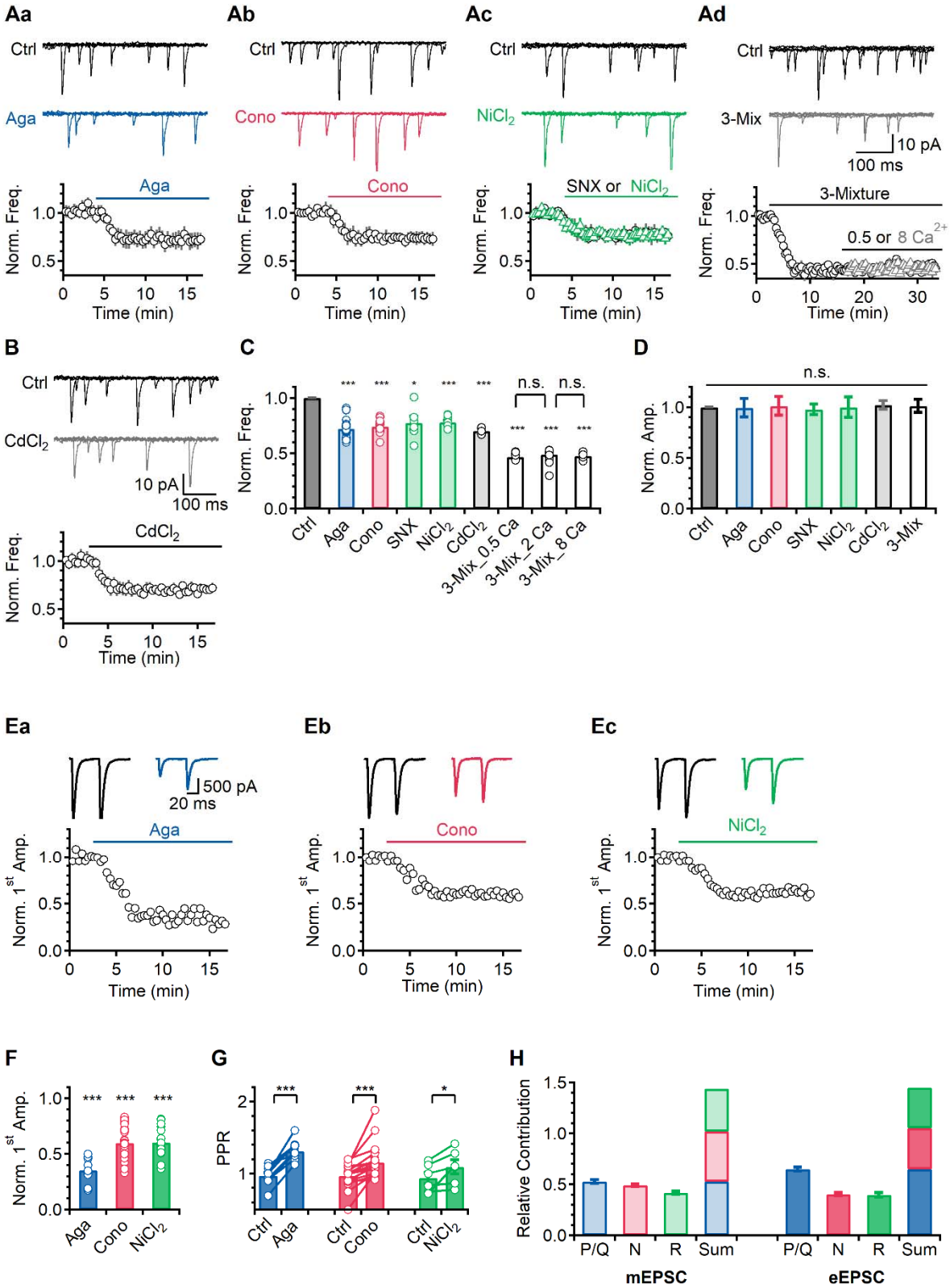
Aa
Ab
Ac
Ad
Ctrl
Aga
Cono
NiCl2
3-Mix
10 pA
100 ms
Norm. Freq.
Time (min)
SNX or NiCl2
3-Mixture
0.5 or 8 Ca2+
B
CdCl2
C
D
n.s.
Norm. Amp.
Ctrl
Aga
Cono
SNX
NiCl2
CdCl2
3-Mix
3-Mix_0.5 Ca
3-Mix_2 Ca
3-Mix_8 Ca
Ea
Eb
Ec
500 pA
20 ms
Norm. 1st Amp.
F
G
H
PPR
Relative Contribution
P/Q
N
R
Sum
mEPSC
eEPSC

Fig. 3.

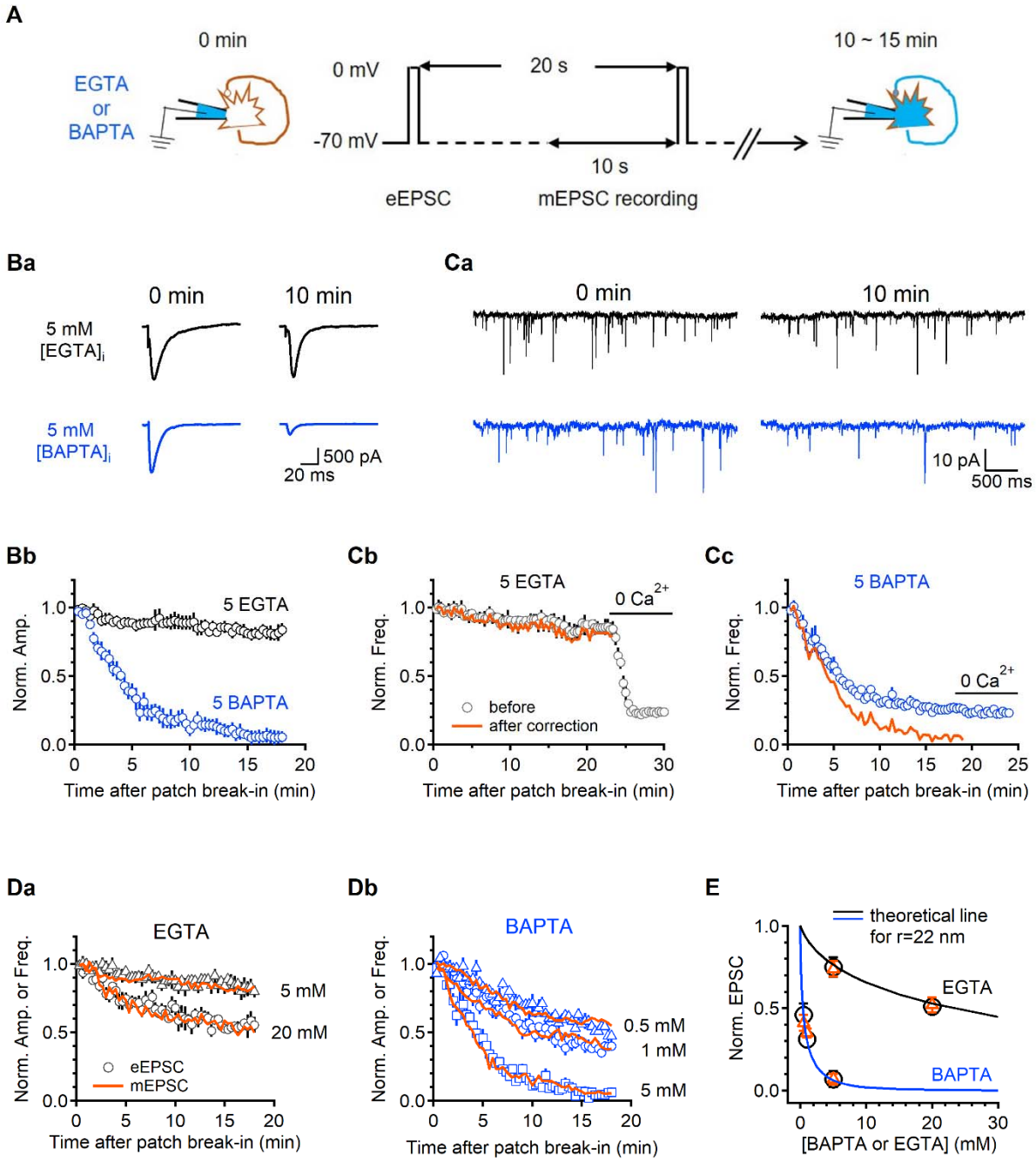
A
0 min
EGTA
or
BAPTA
0 mV
20 s
-70 mV
10 s
eEPSC
mEPSC recording
10 ~ 15 min
Ba
0 min
10 min
5 mM
[EGTA]i
5 mM
[BAPTA]i
500 pA
20 ms
Ca
0 min
10 min
10 pA
500 ms
Bb
5 EGTA
5 BAPTA
Norm. Amp.
Time after patch break-in (min)
Cb
5 EGTA
0 Ca2+
before
after correction
Norm. Freq.
Time after patch break-in (min)
Cc
5 BAPTA
0 Ca2+
Norm. Freq.
Time after patch break-in (min)
Da
EGTA
5 mM
20 mM
eEPSC
mEPSC
Norm. Amp. or Freq.
Time after patch break-in (min)
Db
BAPTA
0.5 mM
1 mM
5 mM
Norm. Amp. or Freq.
Time after patch break-in (min)
E
theoretical line
for r=22 nm
EGTA
BAPTA
Norm. EPSC
[BAPTA or EGTA] (mM)

Fig. 4.

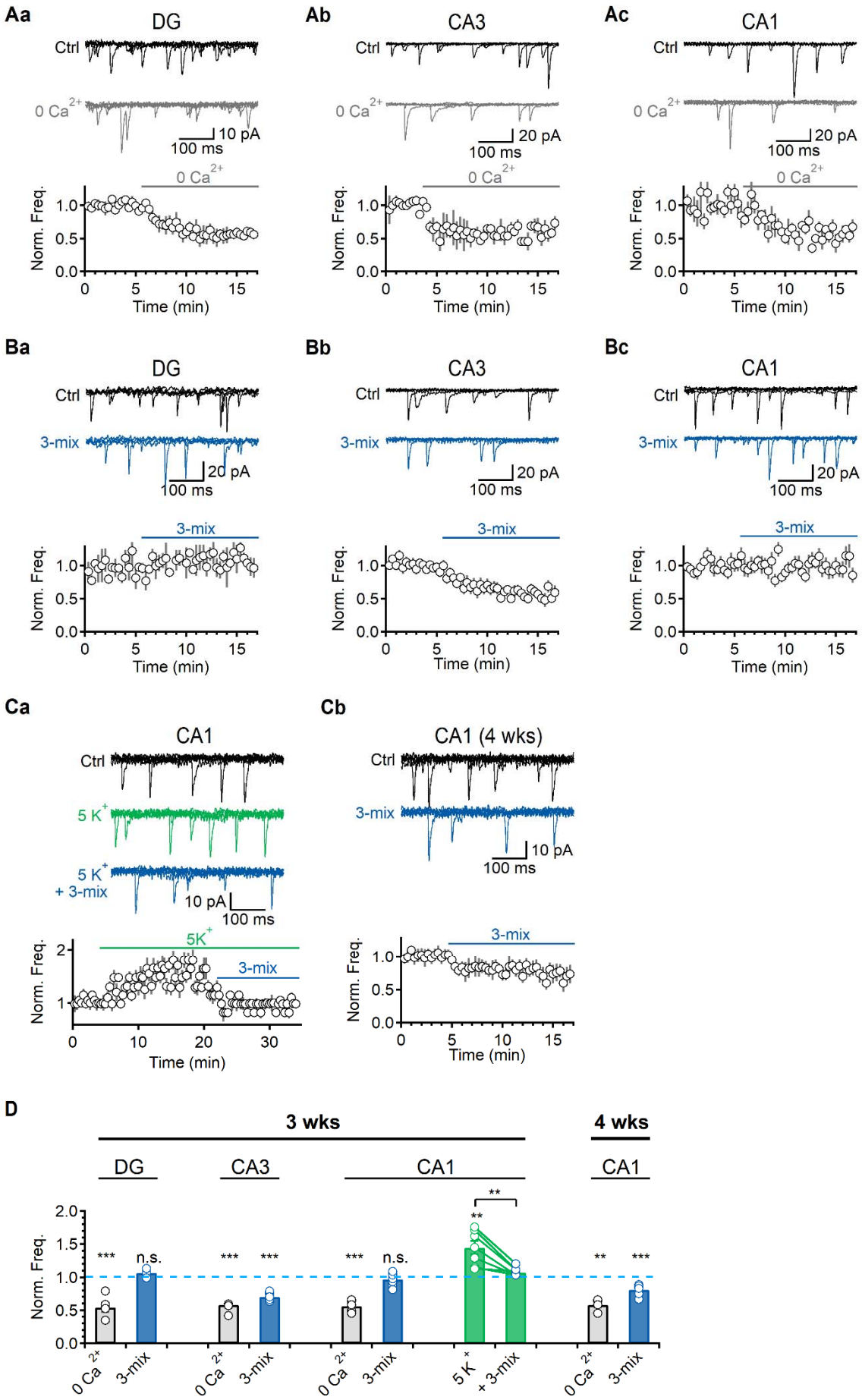
Aa
DG
Ctrl
0 Ca2+
10 pA
100 ms
0 Ca2+
Norm. Freq.
Time (min)
Ab
CA3
Ctrl
0 Ca2+
20 pA
100 ms
0 Ca2+
Norm. Freq.
Time (min)
Ac
CA1
Ctrl
0 Ca2+
20 pA
100 ms
0 Ca2+
Norm. Freq.
Time (min)
Ba
DG
Ctrl
3-mix
20 pA
100 ms
3-mix
Norm. Freq.
Time (min)
Bb
CA3
Ctrl
3-mix
20 pA
100 ms
3-mix
Norm. Freq.
Time (min)
Bc
CA1
Ctrl
3-mix
20 pA
100 ms
3-mix
Norm. Freq.
Time (min)
Ca
CA1
Ctrl
5 K+
5 K+
+ 3-mix
10 pA
100 ms
5K+
3-mix
Norm. Freq.
Time (min)
Cb
CA1 (4 wks)
Ctrl
3-mix
10 pA
100 ms
3-mix
Norm. Freq.
Time (min)
D
3 wks
4 wks
DG
CA3
CA1
CA1
Norm. Freq.
***
n.s.
***
***
***
n.s.
**
**
**
***
0 Ca2+
3-mix
0 Ca2+
3-mix
0 Ca2+
3-mix
5 K+
+ 3-mix
0 Ca2+
3-mix

Fig.5.

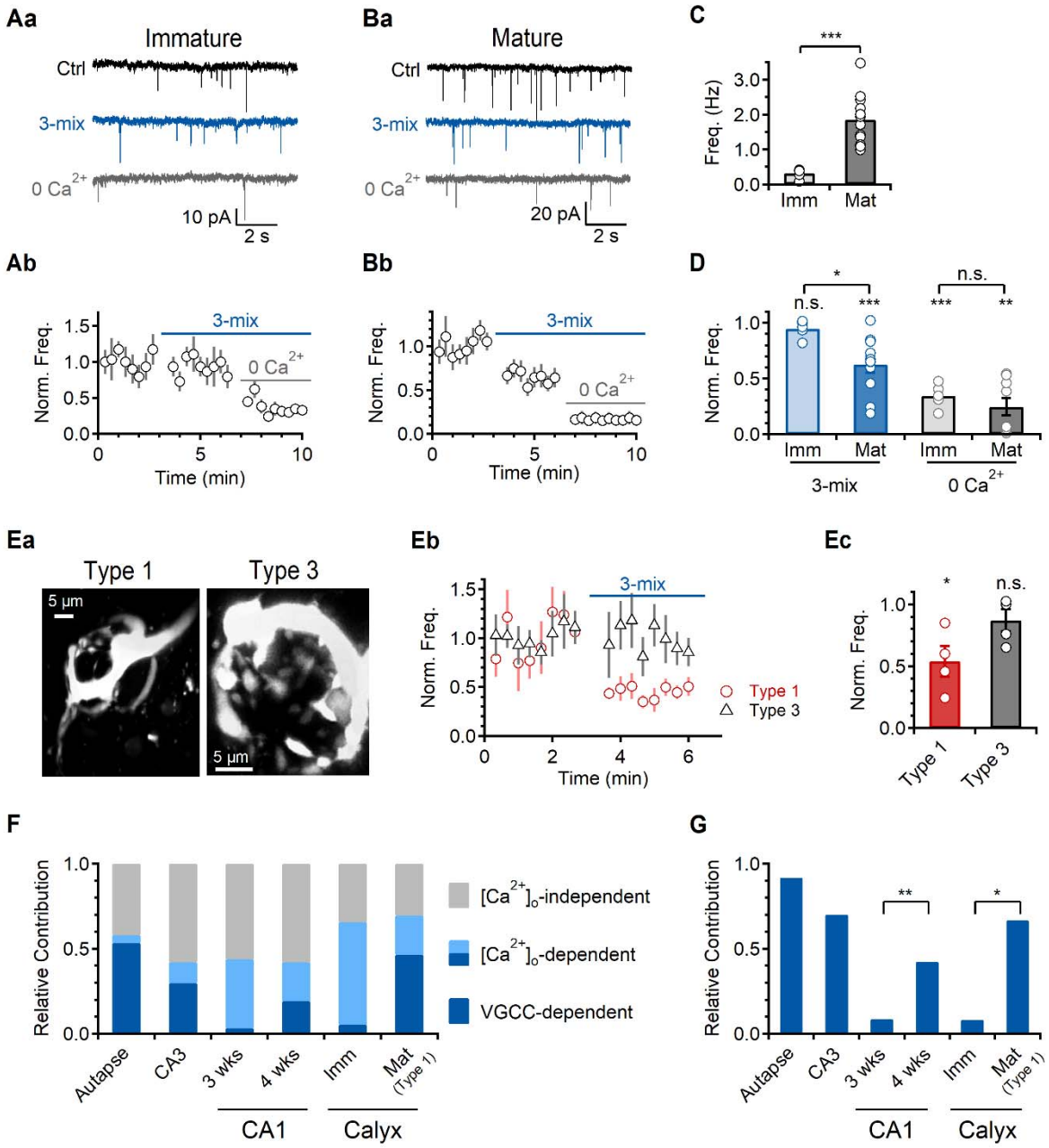
Aa
Immature
Ctrl
3-mix
0 Ca2+
10 pA
2 s
Ba
Mature
Ctrl
3-mix
0 Ca2+
20 pA
2 s
C
***
Freq. (Hz)
3.0
2.0
1.0
0.0
Imm
Mat
Ab
Norm. Freq.
3-mix
0 Ca2+
Time (min)
Bb
Norm. Freq.
3-mix
0 Ca2+
Time (min)
D
*
n.s.
n.s.
***
***
**
Norm. Freq.
Imm
Mat
Imm
Mat
3-mix
0 Ca2+
Ea
Type 1
Type 3
5 µm
5 µm
Eb
Norm. Freq.
3-mix
Type 1
Type 3
Time (min)
Ec
*
n.s.
Norm. Freq.
Type 1
Type 3
F
Relative Contribution
[Ca2+]o-independent
[Ca2+]o-dependent
VGCC-dependent
Autapse
CA3
3 wks
4 wks
Imm
Mat (Type 1)
CA1
Calyx
G
Relative Contribution
**
*
Autapse
CA3
3 wks
4 wks
Imm
Mat (Type 1)
CA1
Calyx